

Transport Properties of Near Surface InAs Two-dimensional Heterostructures

Kaushini S. Wickramasinghe^{1,2}, William Mayer¹, Joseph Yuan¹,

Tri Nguyen³, Lucy Jiao¹, Vladimir Manucharyan², and Javad Shabani¹

¹*Center for Quantum Phenomena, Department of Physics, New York University, NY 10003, USA*

²*Department of Physics, University of Maryland, College Park, MD 20742, USA*

³*Department of Physics, City College of City University of New York, New York City, NY 10031, USA*

(Dated: December 3, 2024)

Two-dimensional electron systems (2DES) confined to the surface of narrowband semiconductors have attracted great interest since they can easily integrate with superconductivity (or ferromagnetism) enabling new possibilities in hybrid device architectures and study of exotic states in proximity of superconductors. In this work, we study indium arsenide heterostructures where combination of clean interface with superconductivity, low density, and spin-orbit coupling can be achieved. We study the magnetotransport as a function of top barrier and density and report clear observation of integer quantum Hall states. We report improved electron mobility reaching up to $44,000 \text{ cm}^2/\text{Vs}$ in undoped heterostructures and well developed integer quantum Hall states starting as low as 2.5 T.

Epitaxial two-dimensional heterostructures containing InAs layers are hypothesized to be suitable systems for spintronics applications¹. Spintronics favors materials like InAs with strong spin orbit interaction (SOC) and large g-factor. Recently, two-dimensional electron systems (2DESs) confined to surface InAs layers have become the focus of renewed theoretical and experimental attention partly because of their potential applications in superconducting quantum computation^{2–4} and realization of topological states of matter^{5,6}. A key feature to these applications is controlled proximity effect with superconductors^{7,8}. InAs is well known to be among a few materials which can interface well with metals and superconductors forming ohmic contacts unlike well known Si and GaAs materials where the interface forms a Schottky barrier. In the past few decades, studies have been focused on high mobility 2DES where the quantum well is placed tens or hundreds of nanometers from the surface^{9–14}. To make proximity devices in these heterostructures, contacts have to be made after etching the top barriers with in-situ ion cleaning. The fabrication difficulties have limited fabrication and test of more complicated Josephson devices¹⁵ since the interface quality/characteristics are proven difficult to finely tune.

Renewed interest in the field of topological superconductivity resulted in development of near surface structures with finite charge distribution overlap with the superconducting contact^{16–18}. Proximity effect can be tuned by the overlap between the wavefunction of the carriers and the superconductor. This can be achieved using growth by insertion of thin layers of low bandgap materials such as InGaAs or gating effect on the semiconductor. Since the 2DES is formed near the surface, the mobility of these structures are naturally lower compared to high-mobility buried structures. In this work we study the magnetotransport properties of near surface InAs quantum wells and for the first time observe integer quantum Hall states. We find that there is an optimum top barrier thickness that preserves reasonable mobility and wavefunction overlap at the surface. Also

spin-orbit interaction measured by weak antilocalization measurement only shows a substantial strength at higher densities. We find replacing InGaAs by InAlAs results in improvement of mobility for comparable thicknesses but the wavefunction overlap near the surface rapidly vanishes.

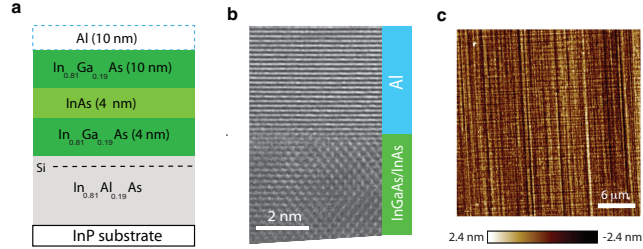


FIG. 1: (Color online) (a) General structure of hybrid Al-InAs surface quantum well. (b) High-resolution transmission microscope image showing that the Al forms a sharp and uniform interface to the InGaAs layer. (c) Atomic force microscopy image shows the surface roughness of about 0.8 nm.

The InAs-Al structure is well suited for the search of the so-called Majorana zero modes, where InAs has a strong SOC and can be well interfaced with Al^{19,20}. In order to probe and establish their unique statistics and eventually move beyond demonstrations of zero bias signatures to braiding^{21,22} and larger-scale Majorana networks^{23,24}, it is likely that a top-down patterning approach will be needed. Growth of large-area 2D Superconductor-Semiconductor systems through Molecular Beam Epitaxy (MBE) can provide the basis for such an approach. Josephson Junctions have been studied¹⁶ and signatures of Majorana fermions have been explored^{17,18} on such 2D hybrid InAs-Al platforms. The question remains how well one can control the 2DES at the surface. For example, if such 2DESs exhibit integer and fractional quantum Hall states one might be able to engineer a system to host parafermion quasiparticle^{25,26}. In this work, we carefully study the electronic transport

of these surface InAs structures. We show we can achieve InAs/InGaAs structures with mobilities reaching 44,000 cm^2/Vs at relatively low density of $3.6 \times 10^{11} \text{ cm}^{-2}$ and observe integer quantum Hall states in magnetic field as low as 2.5 T. The optimized structure provides a semiconducting platform with lower disorder and higher mobility than previously reported^{16,27}.

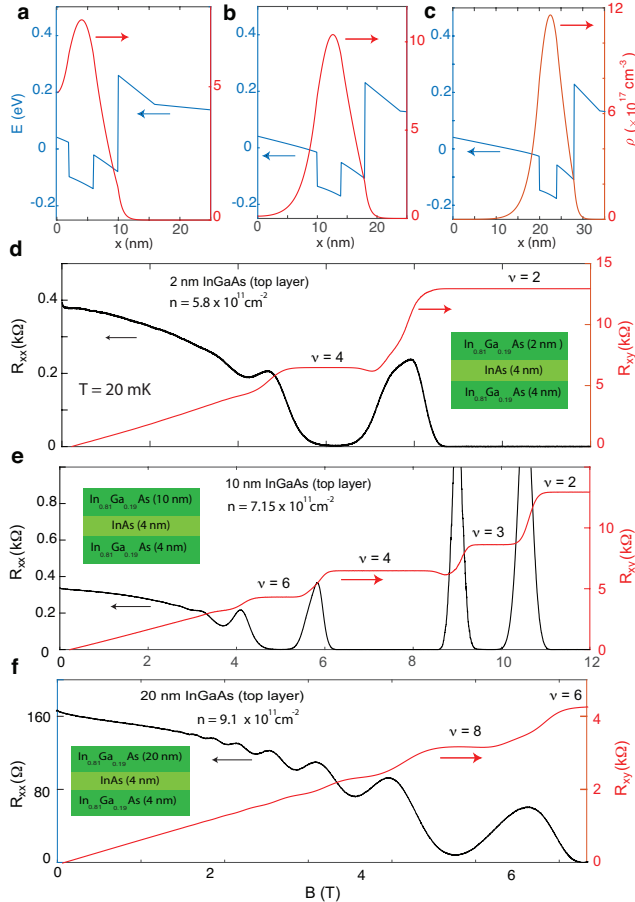


FIG. 2: (Color online) Self consistent Poisson charge distribution calculations for top layers of (a) 2 nm InGaAs, (b) 10 nm InGaAs and (c) 20 nm InGaAs. Magnetotransport and layer structure of InAs quantum wells with top layers of (d) 2 nm InGaAs, (e) 10 nm InGaAs and (f) 20 nm InGaAs.

The samples were grown on semi-insulating InP (100) substrates in a modified Gen II MBE system. The step graded buffer layer, $\text{In}_x\text{Al}_{1-x}\text{As}$, is grown at low temperature to minimize dislocations forming due to the lattice mismatch between the active region and the InP substrate²⁸⁻³⁰. The quantum well consists of a 4 nm layer of InAs grown on a 4 (or 6) nm layer $\text{In}_{0.81}\text{Ga}_{0.19}\text{As}$. This layer helps to recover the InAlAs buffer roughness. We do not observe any improvement in transport mobility when the thickness of this layer is thicker than 4 nm consistent with earlier studies²⁸. A top layer, typically 10 nm of $\text{In}_{0.81}\text{Ga}_{0.19}\text{As}$, is grown on InAs strained quantum well as shown in Fig. 1a. After the quantum well is grown, the substrate is cooled to promote the growth of epitaxial Al

(111)¹⁶. Figure 1b shows a high-resolution transmission electron microscope (TEM) image of this interface between Al and $\text{In}_{0.81}\text{Ga}_{0.19}\text{As}$, with atomic planes of both crystals clearly visible. All samples reported in this paper have had Al thin films grown and thin films of Al were selectively removed, using Al etchant Transene solution type D, for transport studies of the InAs quantum well. The surface roughness of samples does not change with or without Al thin films confirmed by atomic force microscope images. Figure 1c shows a surface topography of a sample with InGaAs top layer on a 34 μm by 34 μm square.

The Fermi level pinning at semiconductor surfaces has been the subject of numerous theoretical and experimental studies. In most semiconductors, such as GaAs, the Fermi level is pinned inside the band gap³¹. It is well known that the surface states in case of InAs can result in a two dimensional electron system³². The electron accumulation is due to pinning of the Fermi level above the conduction band minimum. The position of the pinning level depends on the crystal direction and the surface treatments³³. Experiments on $\text{In}_x\text{Ga}_{1-x}\text{As}$ predicts Schottky barrier height becomes negative, exhibiting an ohmic behavior, for $x > 0.85$ ³⁴. Low temperature transport properties of surface accumulation InAs structures are dominated by surface scattering (low mobility, limited to a 1000-3000 cm^2/Vs) and magnetotransport shows very weak signatures of Shubnikov-de Haas oscillations. Adding a top layer to pure InAs quantum well resolves these issues. Figure 2(d,e,f) shows the longitudinal and Hall resistance traces of a van der Pauw sample with 2, 10 and 20 nm InGaAs top layers with corresponding charge distributions in Figure 2(a,b,c). The effective electron mass of InGaAs at $x = 0.81$ is $m_e = 0.03m_0$, where m_0 is bare mass. This is comparable to effective electron mass of InAs. This results in a quantum well inside a quantum well structure that supports confinement of the wavefunction both in InGaAs and InAs layers while the wavefunction is slowly decaying toward the surface¹⁶. Figure 2d shows the magnetotransport data of a sample with 2 nm InGaAs top layer. As evidenced by charge distribution calculations in Fig. 2a, there is a strong overlap with the surface and suitable for strong coupling of the semiconductor to superconductors. The corresponding longitudinal and Hall data are shown in Fig. 2d. The onset of oscillations for the 2 nm InGaAs top layer sample is near 3 T ($\mu = 6,500 \text{ cm}^2/\text{Vs}$). Increasing the thickness of InGaAs top layer to 10 nm improves the quality as shown in Fig. 2e substantially with mobility increasing to $\mu = 14,400 \text{ cm}^2/\text{Vs}$ and a small but finite overlap of the wavefunction at the surface. Increasing the top layer thickness to 20 nm lowers the visibility of quantum Hall states, slightly lowers the transport mobility to $\mu = 12,570 \text{ cm}^2/\text{Vs}$ and a vanishing wavefunction overlap near the surface. All samples are prepared similarly and measurements are performed at 20 mK. We should also note that a natural choice for top layer is InAlAs. We find that large electron mass and band off-

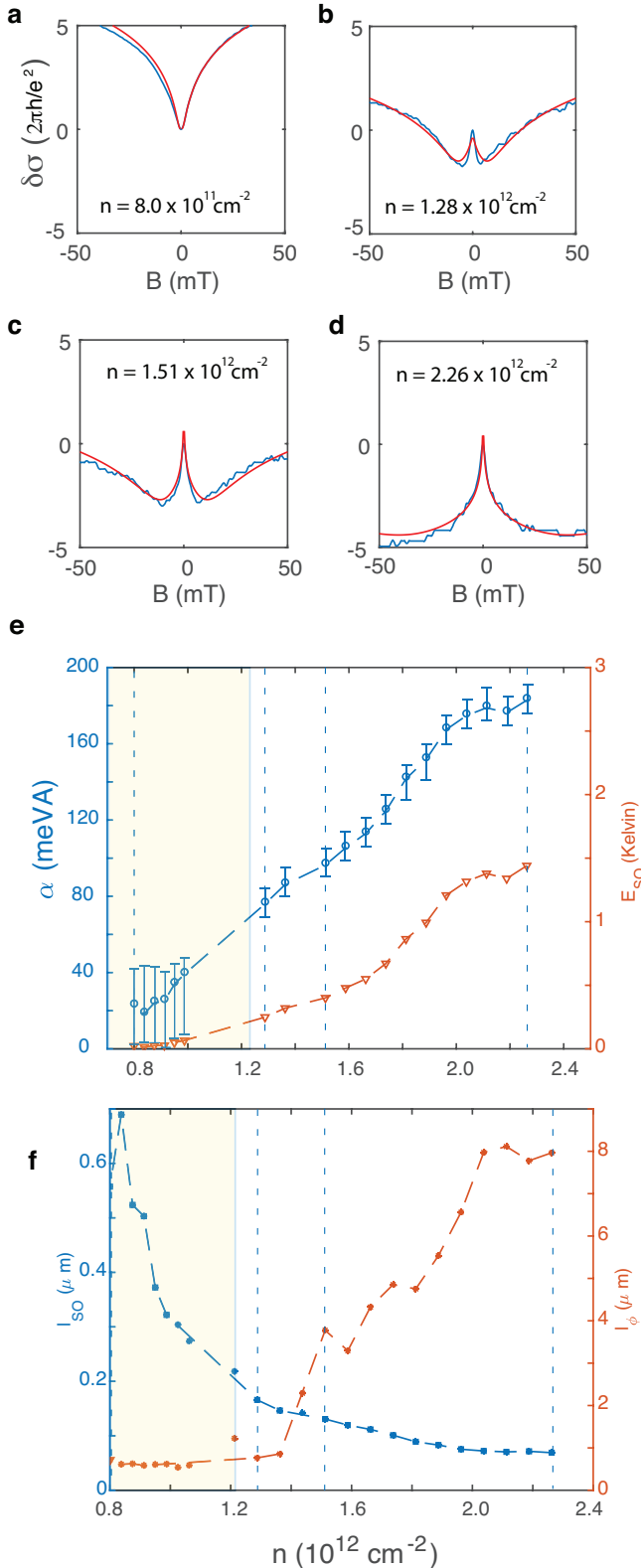


FIG. 3: (Color online) Low magnetic field response of InAs 2DES for densities: (a) $n = 8.0 \times 10^{11} \text{ cm}^{-2}$ (b) $1.28 \times 10^{12} \text{ cm}^{-2}$ (c) $1.51 \times 10^{12} \text{ cm}^{-2}$ (d) $2.26 \times 10^{12} \text{ cm}^{-2}$. The fit using ILP model is shown in red, see text. (e) Rashba SOC parameter, α (left axis) and corresponding spin orbit gap E_{SO} (right axis) as a function of density. (f) Spin orbit length (left axis) and phase coherence length (right axis) as a function of density. Dashed lines corresponds to densities in part (a-d). Shaded regions in parts (e) and (f) denote $l_{SO} \geq l_\phi$ where the fits are no longer valid for extracting spin orbit parameters.

set of ~ 400 meV suppresses the overlap within 5 nm of $\text{In}_{0.81}\text{Al}_{0.19}\text{As}$. Transport properties are reported in Table I.

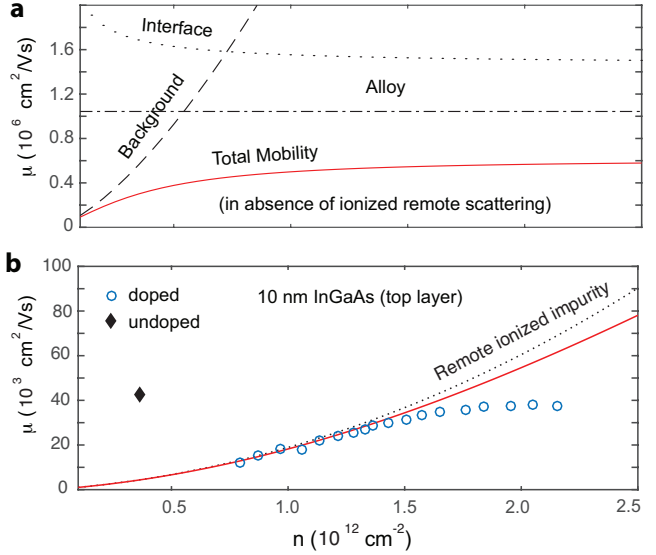


FIG. 4: (Color online) (a) Calculated mobilities from different scattering mechanisms as a function of doping electron density for buried quantum wells. (b) Total theoretical mobility versus measured mobility for surface quantum wells.

Engineering the coupling of the 2DES with surface is an important knob in tuning the proximity effect in Josephson devices. The goal is to keep the finite charge distribution at the surface *in addition to* highest electron mobility and quality of magneto-transport. We have studied several samples with various InGaAs top layer thicknesses and have found that a 10 nm top layer thickness yields the highest quality 2DES as well as good wavefunction overlap at the surface³⁵. The magnetotransport shown in Fig. 2e (with corresponding charge distribution in Fig. 2b). While electron density has not changed much, the quality has increased with onset of oscillations at 2.25 T and $\mu = 14,400 \text{ cm}^2/\text{Vs}$. We also observe a well developed $\nu = 3$ and 6 which were not present in thinner top layers. Recent studies show that having a strong spin-orbit coupling may be compromised in strongly coupled limit, and somewhat weaker interface tunneling may be necessary for achieving optimal proximity⁸ and estimated to be 10 nm in case of $\text{In}_{0.81}\text{Ga}_{0.19}\text{As}$ ¹⁶. For the rest of this paper we focus on properties of structures with 10 nm thick $\text{In}_{0.81}\text{Ga}_{0.19}\text{As}$ top layer.

We next analyze the spin orbit coupling using low field weak antilocalization measurements. These measurements are performed on gated Hall bars fabricated using optical photolithography and wet etch techniques. Fig. 3(a-d) show the measured corrections to conductivity as a function of density (data in blue). At $n = 8.0 \times 10^{11} \text{ cm}^{-2}$, the valley in conductivity shows absence of strong Rashba coupling while with increasing density a peak appears and develops into a strong

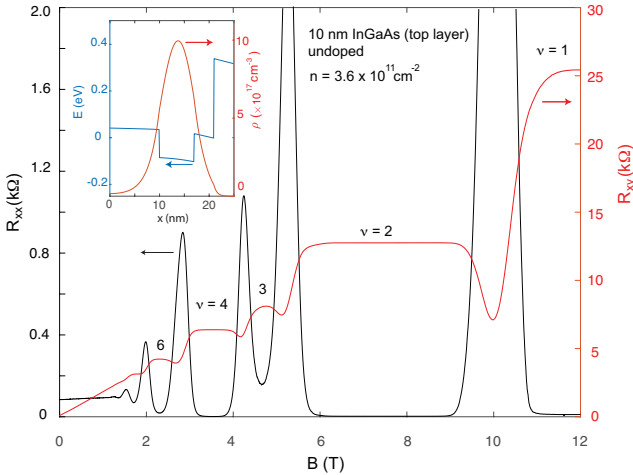


FIG. 5: (Color online) Magnetotransport for an undoped sample in the van der Pauw geometry with top layer of 10 nm In_{0.81}Ga_{0.19}As. (Inset) Corresponding charge-distribution calculated for $n = 3.6 \times 10^{11} \text{ cm}^{-2}$.

peak with increasing density to highest density we probe $n = 2.26 \times 10^{12} \text{ cm}^{-2}$. The data is analyzed using the theory developed by Iordanis, Lyanda-Geller, and Pikus (ILP) for 2DESS³⁶. To reduce the number of free fitting parameters we fixed the value of cubic Dresselhaus SOC, γ as the bulk value of InAs 26.9 eV Å³ calculated from the $\vec{k} \cdot \vec{p}$ theory³⁷. Fitting $\delta\sigma(B)$ over the range $|B| < 50$ mT at $T = 20$ mK yields the linear spin-orbit coupling parameter, α shown in Fig. 3e, and phase-coherence length, l_ϕ shown in Fig. 3f. At high densities, Rashba SOC parameter reaches about 200 meVÅ and spin orbit energy gap, E_{SO} reaches 1.5 K. Similarly, l_ϕ reaches to about 8 μm and l_{SO} to 100 nm with a ratio of $l_\phi/l_{SO} \sim 80$.

The density dependence of the electron mobility can illuminate the various sources contributing to scattering. Fig. 4a shows calculated mobility due to scattering from rough interface, alloy scattering and background doping which are all relevant for deep structures (100 to 200 nm of InAlAs top layer)^{29,30}. The alloy scattering is highly sensitive to the ternary composition, $\mu \sim \frac{1}{x(1-x)}$, is calculated following Ref.³⁸. The background doping, N_B , is deduced based on the observation that undoped deep structures conduct with density range in few 10^{11} cm^{-2} . Based on series of comparison between calculation and measurements we estimate $N_B \sim 10^{16} \text{ cm}^{-3}$. The interface roughness with fluctuation height 0.8 nm adds a cut-off at $1.5 \times 10^6 \text{ cm}^2/\text{Vs}$. Using these values, the total mobility is calculated based on the Matthiessen's rule as shown in red in Fig. 4a. For deep structures, mobility is expected to increase with electron density and saturates around 600,000 cm²/Vs similar to earlier studies²⁹. However recent results in similar structures show higher mobilities can be achieved³⁹ on 120 nm deep structures which may suggest a discrepancy between experiments and alloy scattering model used by Ref.³⁸. In binary InAs quantum wells the electron mobility can reach up to $\mu =$

2.4×10^6 and signatures of fractional quantum Hall state has been observed^{40,41}. Note that these structures can not be interfaced with epitaxial superconductors as near surface structures reported in this paper can.

For surface quantum wells, the situation is different where surface scattering and remote ionized doping, N_d , play major roles. The dependence of the mobility on density of our sample is shown in Fig. 4b. The electron mobility varies between 10,000 cm²/Vs and 40,000 cm²/Vs. The mobility starts to saturate near $1.6 \times 10^{12} \text{ cm}^{-2}$ close to second subband occupation. The data can be fitted by $\mu \sim n^\alpha$, with $\alpha = 0.9$ in density range below $1.6 \times 10^{12} \text{ cm}^{-2}$. Since the contribution of background doping is low in surface quantum wells and exact details of surface impurity scatterings are unknown, we have fitted the data with remote impurity doping⁴² (only the lowest subband is included in the calculation) and found an upper bound $N_d \sim 10^{12} \text{ cm}^{-2}$ with which the data can be reasonably fit (red curve in Fig. 4b). Our surface quantum wells are typically doped by $\sim 10^{12} \text{ cm}^{-2}$ from the back side of the quantum well. Based on these results we studied a van der Pauw sample without back side doping. Figure 5 shows the longitudinal and Hall data at $T = 20$ mK. As expected the electron density is reduced to $n = 3.6 \times 10^{11} \text{ cm}^{-2}$ but electron mobility is enhanced to 44,000 cm²/Vs. Ref.⁴³ reports online on arXiv mobility of $\mu = 54,000 \text{ cm}^2/\text{Vs}$ at a higher density of $n = 8.7 \times 10^{11}$. However they do not present magnetotransport data. In our sample, various integer quantum Hall states are clearly resolved at $\nu = 1, 2, 3, 4, 6, 8$ with onset of oscillation at 1.2 T. We should note that our undoped structures initially did not conduct probably due to surface compensation. Originally during the growth, we would change the indium and aluminum cell temperatures to change the composition during step graded buffer. In all the structures we have presented in this paper, we have kept the Al cell temperature fixed while indium cell temperature has been adjusted during step graded buffer. We found that the optimum arsenic flux and growth temperatures are different and it is only in these structures that undoped surface quantum wells are conducting. The self consistent calculations estimates a carrier density of $\sim 3.3 \times 10^{11} \text{ cm}^{-2}$ assuming all charges are originating from background doping in the barriers as shown in the inset of Fig. 5. This suggests that in optimized structures the compensation is minimal and most of carriers are coming from the barrier and without ionized impurities nearby we can improve the mobility.

In summary, we studied the scattering mechanism of InAs surface quantum wells with InGaAs top layer. In these structures, we find top layer thickness and ionized impurity scattering both affect the mobility. We find at 10 nm top layer and no doping, mobility increases up to 44000 cm²/Vs and observe reduction of onset of oscillation in magneto transport data down to 1.2 T with well developed integer states emerging at 2.5 T.

Our work was supported by US Army research office and DARPA. We thank Kasra Sardashti for fruitful dis-

TABLE I: Summary of InAs surface quantum wells and their transport properties. Top layer material with indium composition of 0.81, barrier thickness in nm: d, Si doping (cm^{-2}): N_d , Electron density (cm^{-2}): n, Mobility: μ , onset of Shubnikov-de Haas (Tesla): B_{on} .

Barrier	d (nm)	N_d (cm^{-2})	n (10^{11}cm^{-2})	μ (cm^2/Vs)	B_{on} (T)
InAlAs	5	10^{12}	10	14,000	1.5
InAlAs	2	10^{12}	6.76	8,500	2
InGaAs	2	10^{12}	5.8	6,500	3
InGaAs	10	10^{12}	7.15	14,400	2.25
InGaAs	10	-	3.6	44,000	1.2
InGaAs	20	10^{12}	10	12,570	1.3

cussions.

¹ Igor Žutić, Jaroslav Fabian, and S. Das Sarma. Spintronics: Fundamentals and applications. *Rev. Mod. Phys.*, 76: 323–410, Apr 2004. doi: 10.1103/RevModPhys.76.323. URL <https://link.aps.org/doi/10.1103/RevModPhys.76.323>.

² Z. Qi, H. Xie, J. Shabani, V. E. Manucharyan, A. Levchenko, and M. G. Vavilov. Controlled-z gate for transmon qubits coupled by semiconductor junctions. *Phys. Rev. B*, 97:134518, 2018.

³ L. Casparis, M. R. Connolly, M. Kjaergaard, N. J. Pearson, A. Kringhoj, T. W. Larsen, F. Kuemmeth, T. Wang, C. Thomas, S. Gronin, G. C. Gardner, M. J. Manfra, C. M. Marcus, and K. D. Petersson. Superconducting gatemon qubit based on a proximitized two-dimensional electron gas. *arXiv:1711.07665*.

⁴ T. W. Larsen, K. D. Petersson, F. Kuemmeth, T. S. Jespersen, P. Krogstrup, J. Nygård, and C. M. Marcus. Semiconductor-nanowire-based superconducting qubit. *Phys. Rev. Lett.*, 115:127001, Sep 2015. doi: 10.1103/PhysRevLett.115.127001. URL <https://link.aps.org/doi/10.1103/PhysRevLett.115.127001>.

⁵ Jason Alicea. New directions in the pursuit of majorana fermions in solid state systems. *Reports on Progress in Physics*, 75(7):076501, 2012. URL <http://stacks.iop.org/0034-4885/75/i=7/a=076501>.

⁶ R. M. Lutchyn, E. P. A. M. Bakkers, L. P. Kouwenhoven, P. Krogstrup, C. M. Marcus, Y. Oreg, and Y. Oreg. Majorana zero modes in superconductor-semiconductor heterostructures. *Nature Reviews Materials*, 3, 2018.

⁷ Jay D. Sau, Sumanta Tewari, and S. Das Sarma. Experimental and materials considerations for the topological superconducting state in electron- and hole-doped semiconductors: Searching for non-abelian majorana modes in 1d nanowires and 2d heterostructures. *Phys. Rev. B*, 85:064512, Feb 2012. doi: 10.1103/PhysRevB.85.064512. URL <https://link.aps.org/doi/10.1103/PhysRevB.85.064512>.

⁸ William S. Cole, S. Das Sarma, and Tudor D. Stanescu. Effects of large induced superconducting gap on semiconductor majorana nanowires. *Phys. Rev. B*, 92:174511, Nov 2015. doi: 10.1103/PhysRevB.92.174511. URL <https://link.aps.org/doi/10.1103/PhysRevB.92.174511>.

⁹ Junsaku Nitta, Tatsushi Akazaki, Hideaki Takayanagi, and Kunihiro Arai. Transport properties in an inas-inserted-channel $\text{in}_{0.52}\text{al}_{0.48}\text{as}/\text{in}_{0.53}\text{ga}_{0.47}\text{as}$ heterostructure coupled superconducting junction. *Phys. Rev. B*, 46:14286–14289, 1992.

¹⁰ H. Kroemer, C. Nguyen, and E. L. Hu. Electronic interactions at superconductor-semiconductor interfaces. *Solid-State Electronics*, 37(4-6):1021, 1994.

¹¹ Hideaki Takayanagi and Tatsushi Akazaki. Temperature dependence of the critical current in a clean-limit superconductor-2deg-superconductor junction. *Solid State Communications*, 96(11):815 – 819, 1995. ISSN 0038-1098. doi: [http://dx.doi.org/10.1016/0038-1098\(95\)00586-2](http://dx.doi.org/10.1016/0038-1098(95)00586-2). URL <http://www.sciencedirect.com/science/article/pii/0038109895005862>.

¹² L. C. Mur, C. J. P. M. Harmans, J. E. Mooij, J. F. Carlin, A. Rudra, and M. Illegems. Experimental indication for supercurrents carried by opened transport channels. *Phys. Rev. B*, 54:R2327–R2330, Jul 1996. doi: 10.1103/PhysRevB.54.R2327. URL <https://link.aps.org/doi/10.1103/PhysRevB.54.R2327>.

¹³ J. P. Heida, B. J. van Wees, T. M. Klapwijk, and G. Borghs. Nonlocal supercurrent in mesoscopic josephson junctions. *Phys. Rev. B*, 57:R5618–R5621, Mar 1998. doi: 10.1103/PhysRevB.57.R5618. URL <https://link.aps.org/doi/10.1103/PhysRevB.57.R5618>.

¹⁴ A. Richter, M. Koch, T. Matsuyama, and U. Merkt. Transport properties of nb/inas(2deg)/nb josephson field-effect transistors. *Supercond. Sci. Technol.*, 12:874, 1999.

¹⁵ C. Lehnert. Nonequilibrium dynamics in mesoscopic superconductor-semiconductor-superconductor junctions. *Thesis, University of California, Santa Barbara*, 1999.

¹⁶ J. Shabani, M. Kjaergaard, H. J. Suominen, Younghyun Kim, F. Nichele, K. Pakrouski, T. Stankevic, R. M. Lutchyn, P. Krogstrup, R. Feidenhans'l, S. Kraemer, C. Nayak, M. Troyer, C. M. Marcus, and C. J. Palmstrøm. Two-dimensional epitaxial superconductor-semiconductor heterostructures: A platform for topological superconducting networks. *Phys. Rev. B*, 93:155402, 2016.

¹⁷ H. J. Suominen, M. Kjaergaard, A. R. Hamilton, J. Shabani, C. J. Palmstrøm, C. M. Marcus, and F. Nichele. Zero-energy modes from coalescing andreev states in a two-

dimensional semiconductor-superconductor hybrid platform. *Phys. Rev. Lett.*, 119:176805, Oct 2017. doi: 10.1103/PhysRevLett.119.176805. URL <https://link.aps.org/doi/10.1103/PhysRevLett.119.176805>.

¹⁸ Fabrizio Nichele, Asbjørn C. C. Drachmann, Alexander M. Whiticar, Eoin C. T. O’Farrell, Henri J. Suominen, Antonio Fornieri, Tian Wang, Geoffrey C. Gardner, Candice Thomas, Anthony T. Hatke, Peter Krogstrup, Michael J. Manfra, Karsten Flensberg, and Charles M. Marcus. Scaling of majorana zero-bias conductance peaks. *Phys. Rev. Lett.*, 119:136803, Sep 2017. doi: 10.1103/PhysRevLett.119.136803. URL <https://link.aps.org/doi/10.1103/PhysRevLett.119.136803>.

¹⁹ Anindya Das, Yuval Ronen, Yonatan Most, Yuval Oreg, Moty Heiblum, and Hadas Shtrikman. Zero-bias peaks and splitting in an al-inas nanowire topological superconductor as a signature of majorana fermions. *Nature Physics*, 8: 887 EP –, 11 2012. URL <http://dx.doi.org/10.1038/nphys2479>.

²⁰ M. T. Deng, S. Vaitiekėnas, E. B. Hansen, J. Danon, M. Leijnse, K. Flensberg, J. Nygård, P. Krogstrup, and C. M. Marcus. Majorana bound state in a coupled quantum-dot hybrid-nanowire system. *Science*, 354 (6319):1557–1562, 2016. ISSN 0036-8075. doi: 10.1126/science.aaf3961. URL <http://science.sciencemag.org/content/354/6319/1557>.

²¹ Jason Alicea, Yuval Oreg, Gil Refael, Felix von Oppen, and Matthew P. A. Fisher. Non-abelian statistics and topological quantum information processing in 1d wire networks. *Nat Phys*, 7(5):412–417, 05 2011. URL <http://dx.doi.org/10.1038/nphys1915>.

²² Bertrand I. Halperin, Yuval Oreg, Ady Stern, Gil Refael, Jason Alicea, and Felix von Oppen. Adiabatic manipulations of majorana fermions in a three-dimensional network of quantum wires. *Phys. Rev. B*, 85:144501, Apr 2012. doi: 10.1103/PhysRevB.85.144501. URL <https://link.aps.org/doi/10.1103/PhysRevB.85.144501>.

²³ Jason Alicea, Yuval Oreg, Gil Refael, Felix von Oppen, and Matthew P. A. Fisher. Non-abelian statistics and topological quantum information processing in 1d wire networks. *Nature Phys.*, 7(5):412–417, 05 2011. doi: 10.1038/nphys1915.

²⁴ Alex Matos-Abiague, Javad Shabani, Andrew D. Kent, Geoffrey L. Fatin, Benedikt Scharf, and Igor Zutic. Tunable magnetic textures: From majorana bound states to braiding. *Solid State Communications*, 262:1 – 6, 2017. ISSN 0038-1098. doi: <https://doi.org/10.1016/j.ssc.2017.06.003>. URL <http://www.sciencedirect.com/science/article/pii/S0038109817301904>.

²⁵ Roger S. K. Mong, David J. Clarke, Jason Alicea, Netanel H. Lindner, Paul Fendley, Chetan Nayak, Yuval Oreg, Ady Stern, Erez Berg, Kirill Shtengel, and Matthew P. A. Fisher. Universal topological quantum computation from a superconductor-abelian quantum hall heterostructure. *Phys. Rev. X*, 4:011036, Mar 2014. doi: 10.1103/PhysRevX.4.011036. URL <https://link.aps.org/doi/10.1103/PhysRevX.4.011036>.

²⁶ David J. Clarke, Jason Alicea, and Kirill Shtengel. Exotic non-abelian anyons from conventional fractional quantum hall states. *Nature Communications*, 4:1348 EP –, 01 2013. URL <http://dx.doi.org/10.1038/ncomms2340>.

²⁷ M. Kjaergaard, H. J. Suominen, M. P. Nowak, A. R. Akhmerov, J. Shabani, C. J. Palmstrøm, F. Nichele, and C. M. Marcus. Transparent semiconductor-superconductor interface and induced gap in an epitaxial heterostructure josephson junction. *Phys. Rev. Applied*, 7: 034029, Mar 2017. doi: 10.1103/PhysRevApplied.7.034029. URL <https://link.aps.org/doi/10.1103/PhysRevApplied.7.034029>.

²⁸ X. Wallart, J. Lastennet, D. Vignaud, and F. Mollot. Performances and limitations of inasinalas metamorphic heterostructures on inp for high mobility devices. *Appl. Phys. Lett.*, 87:043504, 2005.

²⁹ J. Shabani, A. P. McFadden, B. Shojaei, and C. J. Palmstrøm. Gating of high-mobility inas metamorphic heterostructures. *Applied Physics Letters*, 105(26), 2014.

³⁰ J. Shabani, S. Das Sarma, and C. J. Palmstrøm. An apparent metal-insulator transition in high-mobility two-dimensional inas heterostructures. *Phys. Rev. B*, 90: 161303, Oct 2014.

³¹ C. A. Mead and W. G. Spitzer. Fermi level position at metal-semiconductor interfaces. *Phys. Rev.*, 134:A713–A716, May 1964. doi: 10.1103/PhysRev.134.A713. URL <https://link.aps.org/doi/10.1103/PhysRev.134.A713>.

³² D. C. Tsui. Observation of surface bound state and two-dimensional energy band by electron tunneling. *Phys. Rev. Lett.*, 24:303–306, Feb 1970. doi: 10.1103/PhysRevLett.24.303. URL <https://link.aps.org/doi/10.1103/PhysRevLett.24.303>.

³³ L. Canali, J.W.G . Wildoer, O. Kerkhof, and L.P. Kouwenhoven. Low-temperature stm on inas(110) accumulation surfaces. *Appl Phys A*, 66:113, 1998.

³⁴ K. Kajiyama, Y. Mizushima, and S. Sakata. Schottky barrier height of ninaas diodes. *Appl. Phys. Lett.*, 23:458, 1973.

³⁵ Josephson devices fabricated on these structures with 10 nm InGaAs top layer thickness exhibit $I_C R_N \sim 413 \mu V$.

³⁶ S. V. Iordanskii, Y. B. Lyanda-Geller, and G. E. Pikus. *JETP Lett.*, 60:206, 1994.

³⁷ W. Knap, C. Skierbiszewski, A. Zduniak, E. Litwin-Staszewska, D. Bertho, F. Kobbi, J. L. Robert, G. E. Pikus, F. G. Pikus, S. V. Iordanskii, V. Mosser, K. Zekentes, and Yu. B. Lyanda-Geller. Weak antilocalization and spin precession in quantum wells. *Phys. Rev. B*, 53:3912–3924, 1996.

³⁸ D. Chattopadhyay. Alloy scattering in quantum-well structures of semiconductor ternaries. *Phys. Rev. B*, 31:1145–1146, Jan 1985. doi: 10.1103/PhysRevB.31.1145. URL <https://link.aps.org/doi/10.1103/PhysRevB.31.1145>.

³⁹ A. T. Hatke, T. Wang, C. Thomas, G.C. Gardner, and M.J. Manfra. Mobility in excess of $10^6 \text{ cm}^2/\text{v s}$ in inas quantum wells grown on lattice mismatched inp substrates. *Appl. Phys. Lett.*, 111:142106, 2017.

⁴⁰ T. Tschirky, S. Mueller, Ch. A. Lehner, S. Fält, T. Ihn, K. Ensslin, and W. Wegscheider. Scattering mechanisms of highest-mobility InAs/al_xga_{1-x}Sb quantum wells. *Phys. Rev. B*, 95:115304, Mar 2017. doi: 10.1103/PhysRevB.95.115304. URL <https://link.aps.org/doi/10.1103/PhysRevB.95.115304>.

⁴¹ Meng K. Ma, Md. Shafayat Hossain, K. A. Villegas Rosales, H. Deng, T. Tschirky, W. Wegscheider, and M. Shayegan. Observation of fractional quantum hall effect in an inas quantum well. *Phys. Rev. B*, 96:241301, Dec 2017. doi: 10.1103/PhysRevB.96.241301. URL <https://link.aps.org/doi/10.1103/PhysRevB.96.241301>.

⁴² A. Gold. Electronic transport properties of a two-dimensional electron gas in a silicon quantum-well structure at low temperature. *Phys. Rev. B*, 35:723–733, Jan

1987. doi: 10.1103/PhysRevB.35.723. URL <https://link.aps.org/doi/10.1103/PhysRevB.35.723>.

⁴³ Joon Sue Lee, Borzoyeh Shojaei, Mihir Pendharkar, Anthony P. McFadden, Younghyun Kim, Henri J. Suominen, Morten Kjaergaard, Fabrizio Nichele, Charles Marcus, and Chris J. Palmstrø m. Transport studies of epi-al/inas 2deg systems for required building-blocks in topological supercondcutor networks. *arXiv:1705.05049*.